



Applicability of an
integrated plume rise
model

J. Kukkonen et al.

Applicability of an integrated plume rise model for the dispersion from wild-land fires

J. Kukkonen¹, J. Nikmo¹, M. Sofiev¹, K. Riikonen¹, T. Petäjä², A. Virkkula^{1,2},
J. Levula³, S. Schobesberger², and D. M. Webber⁴

¹Finnish Meteorological Institute, Erik Palménin aukio 1, 00101, Helsinki, Finland

²Department of Physics, University of Helsinki, 00014, Helsinki, Finland

³Hyytiälä Forestry Field Station, University of Helsinki, 35500, Korkeakoski, Finland

⁴Integral Science and Software Ltd, 484 Warrington Rd., Culcheth, Warrington WA3 5RA, UK

Received: 16 December 2013 – Accepted: 6 January 2014 – Published: 16 January 2014

Correspondence to: J. Kukkonen (jaakko.kukkonen@fmi.fi)

Published by Copernicus Publications on behalf of the European Geosciences Union.

Title Page

Abstract

Introduction

Conclusions

References

Tables

Figures



Back

Close

Full Screen / Esc

Printer-friendly Version

Interactive Discussion



Abstract

We have presented an overview of a mathematical model, BUOYANT, that was originally designed for the evaluation of the dispersion of buoyant plumes originated from major warehouse fires. The model addresses the variations of the cross-plume integrated properties of a buoyant plume in the presence of a vertically varying atmosphere. The model also includes a treatment for a rising buoyant plume interacting with an inversion layer. We have compared the model predictions with the data of two prescribed wild-land fire experiments. For the SCAR-C experiment in Quinault (US) in 1994, the predicted vertical extents of the plume at maximum plume rise were between 500–800 m and 200–700 m, using two alternative meteorological datasets. The corresponding observed injection heights of the aerosol particles measured using an airborne LIDAR (Light Detection And Ranging) ranged from 250 and 600 m. For the prescribed burning experiment in Hyytiälä (Finland) in 2009, the model predictions were compared with plume elevations and diameters, determined based on particulate matter number concentration measurements on board an aeroplane. The agreement of modelled and measured results was good, provided that one assumes the measured maximum convective heat fluxes as input data for the model. The results demonstrate that in field experiments on wild-land fires, there are substantial uncertainties in estimating both (i) the source terms for the atmospheric dispersion computations, and (ii) the relevant vertical meteorological profiles. The results provide more confidence that cross-plume integrated mathematical models, such as the BUOYANT model, can be used to fairly good accuracy for evaluating the dispersion from major wild-land fires.

1 Introduction

Both fires in warehouses and wild-land fires (the latter include, e.g., heath, moorland, and forest fires) may represent a major hazard or health effect to people and the environment, and the fire plumes may contain a variety of harmful or toxic chemical

GMDD

7, 483–527, 2014

Applicability of an integrated plume rise model

J. Kukkonen et al.

Title Page

Abstract

Introduction

Conclusions

References

Tables

Figures

⏪

⏩

◀

▶

Back

Close

Full Screen / Esc

Printer-friendly Version

Interactive Discussion



Applicability of an integrated plume rise model

J. Kukkonen et al.

Title Page

Abstract

Introduction

Conclusions

References

Tables

Figures

⏪

⏩

◀

▶

Back

Close

Full Screen / Esc

Printer-friendly Version

Interactive Discussion



compounds. The initial vertical distribution of pollutants originating from a fire is controlled by strong updrafts associated with the buoyancy of fire emissions. The pollutants may be transported to the upper part of the atmospheric boundary layer (ABL), to the free troposphere and in some cases to the stratosphere (e.g., Freitas et al., 2007; Sofiev et al., 2012). The composition of effluents from fires and their atmospheric distribution depends on the burned material, processes near the fire, and larger scale atmospheric processes. A crucial near-fire process is the initial plume rise that determines the injection height of the fire plume (e.g., Lioussé et al., 1996; Trentmann et al., 2002).

There are several types of methods for evaluating the injection height of wild-land fire plumes: (i) prescribed vertical emission profiles (e.g., Davison, 2004; Forster et al., 2001 and Lioussé et al., 1996), (ii) semi-empirical plume rise models, such as that presented by Sofiev et al. (2012), and (iii) cross-plume integrated plume-rise models (e.g., Wigley and Slawson, 1971; Martin et al., 1997; Kukkonen et al., 2000). Recently, Devenish et al. (2010) has presented large-eddy simulation (LES) results of buoyant plumes in a crossflow. Comprehensive overviews of buoyant plume models and their history have been presented by, e.g., Devenish et al. (2010) and Jirka (2004).

Many plume rise models currently in use are cross-plume integrated plume-rise models, which consider the conservation of bulk quantities (mass, momentum and enthalpy) integrated over the plume cross-section, with the system of equations closed using an entrainment assumption. The entrainment assumption relates the mean entrainment inflow velocity to the mean plume velocity (Middleton, 1986). Development of these models is based originally on the analysis of Morton et al. (1956), extended to include the effects of vertically varying atmospheric profiles (e.g., Martin et al., 1997).

The plume rise model presented in this paper was originally developed for the EU-funded project “Dispersion from strongly buoyant sources – BUOYANT” (1994–1997), which addressed the atmospheric dispersion of pollutants originated from fires in warehouses and chemical stores. The main objectives of this project were (i) to develop a mathematical model of a plume designed for conditions of very high buoyancy, (ii) to

generate a carefully designed set of experimental data for the high buoyancy, near field region, and (iii) to validate the model against existing data. An overview of this project and its achievements has been presented by Kukkonen et al. (2000) and Ramsdale et al. (1997). More detailed description of the modelling of plume rise and near field dispersion was reported by Martin et al. (1997), and the modelling of the larger scale dispersion was addressed by Nikmo et al. (1997, 1999).

The first aim of this article is to present an overview of the current version of the model called BUOYANT, the original version of which was developed within the above mentioned project. Although the model has originally been developed for the evaluation of fire plumes from warehouses and chemical stores, we also aim to evaluate the model performance for plumes originated from wild-land fires. Major wild-land fires can produce substantially more extensive and intensive fire plumes, compared with characteristic warehouse fires.

The second aim of the article is to evaluate the model predictions against two experimental field datasets of prescribed wild-land fires. These are the “Smoke, Clouds and Radiation – California” experiment, SCAR-C, in Quinault in the US in 1994 (e.g., Kaufman et al., 1996; Hobbs et al., 1996; Gassó and Hegg, 1998) and an experiment in Hyytiälä in Finland in 2009 (Virkkula et al., 2013; Schobesberger et al., 2013). We have also compared the predictions of a simple semi-empirical model of Sofiev et al. (2012) with the measurements of the above mentioned two prescribed fires, and with the predictions of the BUOYANT model.

2 Materials and methods

2.1 Prescribed burn experiments

The SCAR-C experiment in Quinault was selected, as it provides well documented information on the fire, such as fire extent, heat release and emissions, and the measured concentrations and plume dispersion. The experiment in Hyytiälä was selected,

Applicability of an integrated plume rise model

J. Kukkonen et al.

Title Page

Abstract

Introduction

Conclusions

References

Tables

Figures



Back

Close

Full Screen / Esc

Printer-friendly Version

Interactive Discussion



as it also provides detailed information on the fire, and a wide variety of both stationary and mobile ground-based and aircraft-based concentration measurements.

2.1.1 Overview of the SCAR-C experiment in Quinault

“The Smoke, Clouds and Radiation – California”, SCAR-C, experiment was conducted in September 1994 in the Pacific Northwest of the United States (Kaufman et al., 1996; Hobbs et al., 1996; Gassó and Hegg, 1998). It is one of a series of SCAR experiments designed to measure the optical, physical and chemical properties of aerosol particles and their interactions with clouds and radiation. The emphasis of the SCAR-C experiments was to measure the entire process of biomass burning, including ground-based estimates of fuel consumption, airborne sampling of the smoke aerosols and trace gases, and air- and space-borne remote sensing of both the fires and the smoke (Kaufman et al., 1996).

During SCAR-C, four prescribed and eight natural fires were observed and measured (Kaufman et al., 1996). Here we address only the prescribed fire on 21 September in the Quinault Indian Reservation. This burn was typical of large, clear cut, prescribed burns that occur periodically along the coastal lands of the Pacific Northwest (Hobbs et al., 1996).

The fire was a 19.4 ha clear cut burn, fuelled by dry remnants of large western red cedar debris left over from logging. The fire was ignited on 21 September 1994 at about 11:10 LT and immediately burned vigorously, continuing for about six hours. Estimates from ground observations of the ignition pattern and plume indicated that the maximum heat release rate probably occurred between 12:15 and 12:45 LT (Hobbs et al., 1996). At 13:00 the fire was entirely in the smoldering phase. Measurements and estimates of the burn included ground-based fuel consumption, airborne sampling of the particles and trace gases, and remote sensing of both the fire and smoke.

Vertical distribution of smoke particles was derived from the airborne LIDAR measurements between 12:54 and 12:59; these show that most of the smoke particles were between the heights of 250 m and 600 m, some 300 m downwind of the source

Applicability of an integrated plume rise model

J. Kukkonen et al.

Title Page

Abstract

Introduction

Conclusions

References

Tables

Figures



Back

Close

Full Screen / Esc

Printer-friendly Version

Interactive Discussion



(Hobbs et al., 1996). The plume centre line increased in height by about 350 m, as it drifted downwind over a distance of about 25 km. Based on the photographs taken of the smoke originated from the fire, Kaufmann et al. (1996) concluded that the plume was ascended into a layer just under an inversion that was located at the height of 1300 m.

2.1.2 Overview of the prescribed burn in Hyytiälä

The prescribed burning experiment in Hyytiälä in southern Finland was part of both (i) the European Integrated project on “Aerosol Cloud Climate and air Quality Interactions” (EUCAARI, Kulmala et al., 2009) and (ii) the project “Integrated Monitoring and Modelling System for Wildland Fires” (IS4FIRES, Sofiev et al., 2009). A more detailed overview of the experiment and selected results has been presented by Virkkula et al. (2013); the airborne measurements have been discussed in more detail by Schobesberger et al. (2013). The goals of the experiment were to study the aerosol chemical composition and physical characteristics, the concentrations of gaseous compounds, the detection of fires using satellite remote sensing, and the modelling of both fire spreading and atmospheric dispersion of the fire plume.

The burned site had previously been cut clear; some tree trunks, all tree tops and branches were left on the ground. The area of the burned site was 0.806 ha, and it was situated approximately 300–500 m south of the SMEAR II (SMEAR = Station for Measuring forest Ecosystem – Atmosphere Relations) station (Hari and Kulmala, 2005). The experiment was conducted in the morning of 26 June 2009. The burn was ignited at 08:45 LT (UTC +3 h). The flaming phase lasted for 2 h 15 min, the smoldering phase for three hours.

The amount of burned organic material was approximately 46.8 tons (i.e., 60 tons ha⁻¹). Approximately 64 % of the burned material consisted of cut tree material, 32 % of organic litter and humus layer and about 4 % of surface vegetation (Virkkula et al., 2013).

Applicability of an integrated plume rise model

J. Kukkonen et al.

Title Page

Abstract

Introduction

Conclusions

References

Tables

Figures

◀

▶

◀

▶

Back

Close

Full Screen / Esc

Printer-friendly Version

Interactive Discussion



Applicability of an integrated plume rise model

J. Kukkonen et al.

Title Page

Abstract

Introduction

Conclusions

References

Tables

Figures

⏪

⏩

◀

▶

Back

Close

Full Screen / Esc

Printer-friendly Version

Interactive Discussion



The burned area and the location of the measurement stations have been presented in Fig. 1. Stationary measurements were conducted within and in the immediate vicinity of the burned area, at the SMEAR II main building, at the SMEAR II mast, and at the so-called SMEAR II aerosol measurements cottage. In the following, the three latter ones will be called collectively as the SMEAR II stations.

Measurements were conducted on the ground with both stationary and mobile instrumentation, and from a Cessna FR172F aeroplane. Ground-based instrumentation included the SMEAR II stations, together with meteorological and ecological measurements on and around the site (Virkkula et al., 2013). Ground-level measurement of particles and trace gases was also carried out by using a movable research van, and by using portable particle counters at different distances from the burning area.

The airborne measurements addressed also the spatial variability of particle number concentration within the smoke plume. The flights included aircraft ascensions up to an altitude of 4 km and subsequent descents close to the ground level, yielding both vertical and horizontal profiles of the measured parameters. Three measurement flights were conducted, one during the flaming phase, another during the smoldering phase and the third one after the time, at which no smoke was observed at the ground level.

In total 27 smoke plume passages were detected during the first flight. The data was saved at 1 Hz frequency. The ground speed of the aeroplane ranged from 106 to 199 km h⁻¹; this corresponds to a horizontal spatial resolution of approximately 29–55 m for the measured airborne data. The latitude and longitude of the aeroplane was detected using an on board GPS receiver on a time resolution of one second. The altitude was obtained from the pressure altimeter of the aeroplane.

2.2 The modelling of emissions, plume rise and atmospheric dispersion

2.2.1 The overall structure of the BUOYANT model

The model includes treatments (i) for near and intermediate field dispersion of the plume, including the plume rise computations, and (ii) for dispersion after the plume

rise regime. The larger scale dispersion is of particular importance for highly toxic substances. These sub-models constitutes a computer code called BUOYANT, which can be used by hazard analysts to predict the concentration of toxics at different distances from a highly buoyant source, such as a large fire.

5 The sub-model after the plume rise regime has been described in detail by Nikmo et al. (1997, 1999). After the plume rise, but in the vicinity of the source, Gaussian equations are used in both the horizontal and vertical directions. After a specified transition distance, gradient transfer (K-) theory is applied in the vertical direction, while the horizontal dispersion is still assumed to be Gaussian.

10 The near and intermediate dispersion module of the BUOYANT program addresses the behaviour of a buoyant plume in the presence of a wind. The model equations allow for the variation of the relevant atmospheric properties with height. The model also includes a treatment for the case of a rising buoyant plume encountering an inversion layer. Buoyancy is gradually depleted as the plume interacts with the inversion layer, and the plume may run out of buoyancy, while some material is still within the mixing layer. Alternatively, the plume may be sufficiently buoyant to fully penetrate the inversion layer (Martin et al., 1997).

15 In this article, we address in detail only the currently available BUOYANT model treatments for the near and intermediate field dispersion. Compared with the original model version for this regime (Martin et al., 1997), we have revised (i) the equations for the meteorological vertical profiles in stable conditions, to be based on more up-to-date results, and (ii) the criterion for the termination of the plume rise in the model, to be simpler than the original assumptions. Otherwise, the model equations are the same as in the original model formulation. For technical reasons, the model for the near and intermediate field dispersion has also been coded again at the Finnish Meteorological Institute.

20 The model contains three parameters that need to be experimentally determined. However, we have simply used the values that were determined previously in wind

GMDD

7, 483–527, 2014

Applicability of an integrated plume rise model

J. Kukkonen et al.

Title Page

Abstract

Introduction

Conclusions

References

Tables

Figures

⏪

⏩

◀

▶

Back

Close

Full Screen / Esc

Printer-friendly Version

Interactive Discussion



tunnel experiments (e.g., Kukkonen et al., 2000). The model contains no freely adjustable parameters, and it has not been fitted to the measured data.

2.2.2 Previous evaluations of the BUOYANT model against experimental data

The plume rise sub-model of the original version of the BUOYANT model has been evaluated against the experimental data generated by the University of Hamburg in their wind tunnel facility. The results of the model evaluation in the wind tunnel facility have been presented by Liedtke and Schatzmann (1997), and reviews of this model evaluation by Martin et al. (1997) and Kukkonen et al. (2000). The wind tunnel simulations were conducted both in unstratified boundary layers and in the presence of an elevated inversion. The overall agreement of model predictions and measured data was good. One of the experimental data sets was used to determine best estimates for three parameters, which appear in the buoyant plume rise model (Martin et al., 1997).

The BUOYANT sub-model after the plume rise regime has been tested against the Kincaid experimental field data (Olesen, 1995). The average agreement of the predictions and the data was reasonably good (Kukkonen et al., 2000).

Recently, Sofiev et al. (2012) have compared the BUOYANT plume rise model predictions against a dataset collected using the Multi-angle Imaging SpectroRadiometer (MISR) Plume Height Project (Diner et al., 1998; Mazzone et al., 2007). In this project, measured data was collected for about 2000 fire plumes in North America and Siberia. The predictions of the BUOYANT model (the same model version as used in this study), and those obtained using a semi-empirical plume rise model, were compared with remote-sensing observations of the plume top. Overall, the BUOYANT model provided for fairly reliable predictions, in comparison with the measured data. E.g., more than half of the model predictions were within the uncertainty of the observations (± 500 m), compared with the measured values. However, the model slightly underestimated the observed plume tops; one possible reason for this could be that the model does not allow for the influence of water vapour condensation.

Applicability of an integrated plume rise model

J. Kukkonen et al.

Title Page

Abstract

Introduction

Conclusions

References

Tables

Figures



Back

Close

Full Screen / Esc

Printer-friendly Version

Interactive Discussion



2.2.3 Modelling of the mass and heat fluxes of fires

The mass flux is determined with a relative simple integral approach. Assuming that plume gases have similar specific heat capacities and molecular mass values to hot air, the mass flux can be estimated simply as (e.g., Fisher et al., 2001)

$$q = vA\rho, \quad (1)$$

where v is the vertical velocity of the gas mixture, A is the horizontal area of the source and ρ is the density of air. The convective heat flux is modelled as

$$Q_c = c_p q (T - T_{\text{amb}}), \quad (2)$$

where c_p is the specific heat of gas, T is the temperature of the gas and T_{amb} is the ambient temperature.

2.2.4 Modelling of the plume rise and near field dispersion

The BUOYANT model is applicable for steady state buoyant plumes within a vertically varying atmosphere, i.e., wind speed, ambient temperature, pressure and density vary with height. The atmosphere surrounding the plume is assumed to be undisturbed by the source, i.e., its characteristics are not affected by the heat released from the source.

The model also includes a treatment for the plume encountering a temperature inversion above the atmospheric boundary layer. Buoyancy is gradually depleted as the plume interacts with the inversion layer, and the plume may run out of buoyancy while some of the material is still within the mixing layer. Alternatively, the plume may be sufficiently buoyant to fully penetrate the inversion layer.

Vertical profiles of wind speed, temperature, pressure and density in the atmosphere

The vertical structure of the atmosphere is assumed to comprise three distinct layers; atmospheric boundary layer (ABL), capping inversion layer and upper layer. In the

lowest layer (ABL) the vertical variations of wind speed (u) and potential temperature (θ) are assumed to be described with profiles based on the Monin–Obukhov similarity theory (e.g., Garratt, 1994),

$$u(z) = \frac{u_*}{\kappa} \left(\ln \left(\frac{z}{z_0} \right) - \psi_m(\xi) + \psi_m(\xi_0) \right), \quad (3)$$

$$\theta(z) - \theta(z_{0h}) = \frac{\theta_*}{\kappa} \left(\ln \left(\frac{z}{z_{0h}} \right) - \psi_h(\xi) + \psi_h(\xi_{0h}) \right), \quad (4)$$

where z is the height above ground, u_* is the friction velocity, κ is the von Karman constant, z_0 is the roughness length of momentum, ψ_m and ψ_h are the influence functions of mass and heat, $\xi = zL^{-1}$ is the dimensionless height (thermal stability parameter), L is the Monin–Obukhov length, $\xi_0 = z_0L^{-1}$, θ_* is the temperature scale, z_{0h} is the roughness length of heat and $\xi_{0h} = z_{0h}L^{-1}$.

For the influence functions in unstable conditions ($L < 0$), we apply the commonly accepted expressions (usually referred to as Businger–Dyer profiles)

$$\psi_m(\xi) = 2 \ln \left(\frac{1+Y}{2} \right) + \ln \left(\frac{1+Y^2}{2} \right) - 2 \tan^{-1} Y + \frac{\pi}{2}, \quad (5)$$

$$\psi_h(\xi) = 2 \ln \left(\frac{1 + (1 - \gamma_h \xi)^{1/2}}{2} \right), \quad (6)$$

where $Y = (1 - \gamma_m \xi)^{1/4}$ and for the constants we apply the values proposed by Brutsaert (1982), i.e. $\gamma_m = \gamma_h = 16$.

Applicability of an integrated plume rise model

J. Kukkonen et al.

Title Page	
Abstract	Introduction
Conclusions	References
Tables	Figures
◀	▶
◀	▶
Back	Close
Full Screen / Esc	
Printer-friendly Version	
Interactive Discussion	



For stable conditions ($L > 0$), we use the expressions proposed by Beljaars and Holtslag (1991)

$$\psi_m(\xi) = -a\xi - b\left(\xi - \frac{c}{d}\right)\exp(-d\xi) - \frac{bc}{d}, \quad (7)$$

$$\psi_h(\xi) = -\left(1 + \frac{2}{3}a\xi\right)^{3/2} - b\left(\xi - \frac{c}{d}\right)\exp(-d\xi) - \frac{bc}{d} + 1, \quad (8)$$

where the constants $a = 1$, $b = 0.667$, $c = 5$ and $d = 0.35$. The previous version of the BUOYANT model used wind speed and temperature profiles according to van Ulden and Holtslag (1985) and Paulson (1970).

In the upper layer, the wind speed is assumed to be constant (representing the geostrophic flow), while within the inversion layer the wind speed is assumed to change with constant gradient from its value at the top of the ABL to the geostrophic value (the constant value within the upper layer). The inversion layer has a constant potential temperature gradient. The upper layer may have a potential temperature gradient that is zero or positive (albeit smaller than in the inversion layer).

Pressure and density of air are obtained by employing the hydrostatic assumption, i.e. force of gravity is balanced by the vertical component of the atmospheric pressure gradient force (Martin et al., 1997). The turning of the wind with height has been ignored, i.e., the plume centre line trajectory is assumed to lie in a vertical plane. The model also does not allow for the influence of atmospheric humidity.

The fluxes of mass, momentum and heat of the plume

For readability, we present here an overview of the plume equations within a varying atmosphere. For a more detailed description, the reader is referred to Martin et al. (1997).

The source is assumed to be circular and horizontal. The gases at the source consist of a mixture of dry air and contaminant gas. Changes of phase (condensation of vapour or evaporation of liquid) are not handled. The plume is allowed to have buoyancy both

Applicability of an integrated plume rise model

J. Kukkonen et al.

Title Page

Abstract

Introduction

Conclusions

References

Tables

Figures

⏪

⏩

◀

▶

Back

Close

Full Screen / Esc

Printer-friendly Version

Interactive Discussion



by virtue of having a higher temperature than its surroundings and because it contains a gas of different molecular weight than that of air. The mixture is assumed to have only vertical velocity at the source. The source is assumed to persist for a sufficient length of time so that the plume achieves a steady state behaviour.

The plume is assumed to remain axially symmetric as it rises. The radial variation of quantities of interest will be assumed to be described by a “top-hat” profile. The contaminant gas is assumed not to react with the air or change its state from gas. The ordinary differential equations describing the plume will be derived by considering the rate of change of (integral) fluxes along the plume. These equations include those for the fluxes of mass, momentum and heat, closed by an entrainment assumption.

The mass flux change due to entrainment of air is given by

$$\frac{dq}{ds} = 2\pi r \rho_a u_e, \quad (9)$$

where s is the distance along the plume centre line trajectory, r is the radius of the plume in the direction normal to the plume axis, ρ_a is the density of ambient air and u_e is the entrainment velocity.

The model employs an entrainment closure approach that distinguishes between the separate contributions of transverse shear (leading to jet, plume, or wake internal flow dynamics) and of azimuthal shear mechanisms (leading to advected momentum puff or thermal flow dynamics), respectively

$$u_e = \alpha_1 \left(\frac{\rho}{\rho_a} \right)^{0.5} |u - u_w \sin(\alpha)| + \alpha_2 \left(\frac{\rho}{\rho_a} \right)^{0.5} u_w \cos(\alpha), \quad (10)$$

where α_1 and α_2 are the along and cross plume air entrainment coefficients, respectively, ρ is the mean density of the plume, u is the mean velocity along the plume centre line, u_w is the wind speed and α is the angle between the direction of the plume and the vertical. We have applied the values for the air entrainment coefficients determined based on wind tunnel experiments, i.e., $\alpha_1 = 0.08$ and $\alpha_2 = 0.7$ (Martin et al., 1997).

Applicability of an integrated plume rise model

J. Kukkonen et al.

Title Page	
Abstract	Introduction
Conclusions	References
Tables	Figures
⏪	⏩
◀	▶
Back	Close
Full Screen / Esc	
Printer-friendly Version	
Interactive Discussion	



Applicability of an integrated plume rise model

J. Kukkonen et al.

Title Page

Abstract

Introduction

Conclusions

References

Tables

Figures

⏪

⏩

◀

▶

Back

Close

Full Screen / Esc

Printer-friendly Version

Interactive Discussion



The first term on the right-hand side of the Eq. (10) represents the entrainment of air due to the velocity difference between the plume and the air along the plume direction. This term is referred to as along plume entrainment. The second term represents cross plume entrainment, which is zero in calm air. The entrainment assumption takes the same form whether the plume is rising vertically or is close to horizontal (bent-over plumes).

The form of the entrainment terms is after Ricou and Spalding (1961). This differs from the Morton and Taylor entrainment velocity (Morton et al., 1956), by inclusion of the square root of the density ratio. The selection between these two entrainment models is important for plumes that have a density that differs substantially from ambient air density. However, there is no conclusive experimental evidence regarding which of these two models would be preferable.

The rate of change of horizontal (ϕ_x) and vertical (ϕ_z) momentum fluxes are

$$\frac{d\phi_x}{ds} = \frac{dq}{ds} u_w \quad (11)$$

$$\frac{d\phi_z}{ds} = \frac{\pi r^2 g (\rho_a - \rho)}{1 + k_v \sin(\alpha)},$$

where g is the acceleration due to gravity and k_v is an adjustable coefficient (of order one). The term including k_v is called the added mass term. The denominator of the vertical momentum flux equation is a term for added mass included to account for the plume having to push air out of the way as it rises. However, there is some controversy about the term involving k_v , which is defined by analogy to the behaviour of a line thermal (Martin et al., 1997). We have applied by default the value $k_v = 1.0$, and some model sensitivity runs were also performed by assuming $k_v = 0.0$. There is no drag term in the momentum equation.

The change of horizontal and vertical excess momentum fluxes (due to the vertical gradient of the wind speed) are

$$\frac{d\phi_x^e}{ds} = -\frac{\overline{du_w}}{dz} q \cos(\alpha) \quad (12)$$

$$\frac{d\phi_z^e}{ds} = \frac{d\phi_z}{ds},$$

5 where $\overline{du_w/dz}$ is the mean representative wind speed gradient. The plume equations are derived on the assumption that the gradients in ambient atmospheric properties are constant across the plume cross-section.

In considering the behaviour of a rising plume contacting an elevated inversion, the mean representative wind speed gradient is an area-weighted average defined as

$$\overline{\frac{du_w}{dz}} = \sum_{i=1}^3 \left(\frac{du_w}{dz} \right)_i f_i, \quad (13)$$

where $(du_w/dz)_i$ is a representative value for the portion of plume within the i th layer and f_i is the fraction of plume cross-sectional area lying in the i th layer.

The rate of change of the excess enthalpy flux is given by

$$\frac{dH^e}{ds} = -\frac{\overline{d\theta_a}}{dz} \cos(\alpha) c_{pa} \left(q + \left(\frac{c_{pg}}{c_{pa}} - 1 \right) S \right), \quad (14)$$

15 where θ_a is the potential temperature of ambient air, c_{pa} and c_{pg} are the specific heat capacities of air and released substance, respectively, and S is the constant contaminant flux. The mean representative gradient of θ_a is defined analogously to the mean
 20 wind speed gradient, Eq. (13). The trajectory of the plume is obtained from the following

simple kinematic relationships

$$\begin{aligned}\frac{dx}{ds} &= \sin(\alpha) \\ \frac{dz}{ds} &= \cos(\alpha),\end{aligned}\tag{15}$$

where x is the downwind distance from the source.

5 The model has three experimentally adjustable parameters: along (α_1) and cross (α_2) plume entrainment coefficients, and the coefficient for the added mass term (k_v). We have set the values of the plume entrainment coefficients based on wind tunnel measurements, and a default value of unity has been used for the added mass term. The buoyant plume model has no remaining adjustable parameters.

10 2.2.5 Criterion for the termination of plume rise

The determination of the final plume rise presents a number of challenges, as discussed by, e.g., Devenish et al. (2010). The observed behaviour of a buoyant plume shows that in some cases the plume simply approaches a final rise height at some distance downwind. At this distance, both the buoyancy force and the vertical momentum
15 vanish. The same behaviour is demonstrated by model simulations.

However, in some other situations, model computations show that during the initial rise the buoyancy force acting on it may fall to zero. The plume does not immediately stop rising, since it will have some upward momentum. The upward momentum will eventually vanish at maximum rise height, at which time a negative buoyancy may
20 cause the plume to descend. In principle, the plume executes a damped harmonic oscillation, damped because the mass flux is assumed to continue increasing. The plume oscillates with decaying amplitude as it settles down to its asymptotic height. The height, at which the buoyancy first becomes zero, is termed here the equilibrium height.

Applicability of an integrated plume rise model

J. Kukkonen et al.

Title Page

Abstract

Introduction

Conclusions

References

Tables

Figures

⏪

⏩

◀

▶

Back

Close

Full Screen / Esc

Printer-friendly Version

Interactive Discussion



Applicability of an integrated plume rise model

J. Kukkonen et al.

Title Page

Abstract

Introduction

Conclusions

References

Tables

Figures

⏪

⏩

◀

▶

Back

Close

Full Screen / Esc

Printer-friendly Version

Interactive Discussion



The equilibrium height can be expected to provide an estimate of the asymptotic height. Also available observations support the use of the equilibrium height (Briggs, 1975; Martin et al., 1997). According to the computations of Martin et al. (1997), the asymptotic height attained by a bent-over plume rising in a layer of constant positive vertical potential temperature gradient is only a few per cent higher than the equilibrium height. They therefore concluded that the asymptotic height of the plume is very close to the equilibrium height, and suggested the equilibrium height to be a suitable height to terminate the calculation.

In the current model version, we have adopted simply to use the equilibrium height as the final rise height of the plume. The previous model version included two additional criteria for the termination of the rise. These are (i) to terminate, if the plume as a whole has penetrated the inversion layer, and (ii) to terminate, if the horizontal speed of the plume is close to the ambient wind speed. The current model version does not include these two criteria, as we considered it relevant to consider also the plume behaviour after a possible penetration of an inversion layer, and in case of very light wind speeds or calm conditions.

2.2.6 The model input data and the numerical solution

The model requires input concerning the meteorological conditions, the source term and the model parameters. The meteorological input includes the following: the Monin–Obukhov length, the height of mixing layer, the roughness lengths of heat and momentum transfer, the air temperature, the pressure and wind speed at a reference height, the height of the inversion layer (above the mixing layer), the potential temperature gradient within the inversion layer, and wind speed and potential temperature gradient above the inversion layer.

Information on the source term includes the following: the source radius, the source height above the ground, the temperature of the released mixture of contaminant gas (and particles) and air, the mass flux of this mixture, the mass fraction of the released gas, and the molecular weight and heat capacity of the released gas. The model

fire. The data has been extracted from the data portal of the ECMWF (ERA 40, 2013). We have selected the time instant of the ERA-40 data at 11:00 LT (18:00 UTC) on 21 September 1994. In the following, we will express all times as local time.

The vertical wind speed and temperature profiles applied by the model have been presented in Eqs. (3) and (4). However, the relevant atmospheric stability parameters, such as, e.g., the Monin–Obukhov length, have not been reported. We have therefore evaluated the Monin–Obukhov length using an approximate analytical method presented by Blümel (2000), which is based on a relationship between the stability parameter ξ and the bulk Richardson number. We used as input values for this method the measured values of temperature and wind speed at two height levels. The roughness lengths of momentum and heat transfer were also evaluated based on the reported experimental data.

The atmospheric temperature and wind speed profiles measured on-site on board the Convair aeroplane, and based on the ERA-40 analysed data have been presented in Fig. 2a and b. The measured on-site vertical profiles have been obtained by combining airborne measurements and radiosonde observations. The modelled profiles were evaluated in both cases based on Eqs. (3) and (4), and the measured data.

According to both assessment methods, the on-site and ERA-40 evaluations, there was an elevated inversion with a magnitude of about 3°C. This was located at the heights from approximately 320 m to 600 m (with a lapse rate of 1.2°C/100 m) or from 200 m to 400 m (with a lapse rate of 1.7°C/100 m), according to the modelled profiles fitted to the on-site and ERA-40 evaluations, respectively. This difference in the evaluated altitudes of the inversions could have a substantial influence on the modelled plume behavior. As the plume will penetrate an inversion layer, the buoyancy of the modelled plume will be correspondingly decreased.

These two meteorological evaluations were also significantly different for the profiles of the wind speed, both regarding the original data and the modelled profiles fitted to the data. The wind speeds evaluated by ERA-40 were substantially higher, compared

GMDD

7, 483–527, 2014

Applicability of an integrated plume rise model

J. Kukkonen et al.

Title Page

Abstract

Introduction

Conclusions

References

Tables

Figures

⏪

⏩

◀

▶

Back

Close

Full Screen / Esc

Printer-friendly Version

Interactive Discussion



with the on-site aeroplane data. If the horizontal wind speed is larger, the modelled plume trajectory will be more strongly bent to the wind direction.

Part of the differences of the evaluations using the two methods could be caused by the spatial representativity of the ERA-40 data used. The selected data point may be representative for more inland conditions, compared with the prescribed burning site.

3.1.2 Evaluation of the source term for the dispersion computations

As input values of the BUOYANT model, we will need to know the following source properties: (i) convective energy release from the fire, (ii) the physical extent of the fire and (iii) the fire temperature. It can be shown by numerical simulations (not shown here) using the BUOYANT model that the convective energy release is the most important source parameter, in terms of the final plume rise.

Heat release rate over time for the Quinault burn has been estimated by Hobbs et al. (1996), using the Emission Production Model (EPM; Sandberg and Peterson, 1984). The EPM model takes into account the loading, consumption, and moisture of different fuels and the duff (the latter is defined to be the decayed material on the forest floor), and also accounts for the different phases of the fire (flaming and smoldering). The EPM model evaluates as model output, among other things, the total heat released per time (energy flux) by a fire. The model can be used for evaluating the time-dependent release of energy originated from the fire, and the emissions of fine particulate matter (aerodynamic diameter $< 2.5 \mu\text{m}$) and some trace gases (CO , CO_2 and CH_4).

The temporal maximum of the total heat release rate predicted by the EPM model was about 6.5 GW (Hobbs et al., 1996); this occurred at 13:05. However, only the convective energy release is needed for the buoyant plume computations (not the radiative contribution and the heat conduction to the ground). The total heat release rate has therefore been multiplied by a factor of 0.55 (Trentmann et al., 2002). The value of this factor depends on several characteristics of the fuel; the value used here is simply in the middle of the commonly accepted range from 0.4 to 0.8 (Trentmann et al., 2002).

Applicability of an integrated plume rise model

J. Kukkonen et al.

Title Page

Abstract

Introduction

Conclusions

References

Tables

Figures

◀

▶

◀

▶

Back

Close

Full Screen / Esc

Printer-friendly Version

Interactive Discussion



We have therefore selected as input for the BUOYANT model simulations the maximum convective heat flux, 3.6 GW.

However, the maximum heat release rate probably occurred somewhat earlier, between 12:15 and 12:45, based on the estimates from ground observations of the ignition pattern and the plume. At that time, a maximum area was in combustion (Hobbs et al., 1996). Clearly, the evaluation of the optimally representative convective heat flux includes many uncertainties.

The Geostationary Operational Environmental Satellite (GOES)-8 Automated Biomass Burning Algorithm (ABBA) was used to estimate the average fire temperature range from 586 to 626 K, from 12:45 to 14:32 (Menzel and Prins, 1996). We have selected the value of 600 K for the fire temperature. The maximum fire size (during both flaming and smoldering) was evaluated to be about 0.17 km², based on ground observations; this occurred at 12:15 (Menzel and Prins, 1996). We have selected this value (0.17 km²) for the source area.

3.1.3 Comparison of the predictions of the BUOYANT model against observations and previous modelling studies

The modelled plume altitudes have been presented in Fig. 3, applying both meteorological options. The plume has a substantially lower injection height and a shallower trajectory for the ERA-40 meteorology case, as compared with the on-site meteorology case. This is due both to (i) the lower altitude of the inversion layer and (ii) the substantially higher wind speeds for the ERA-40 case (cf. Fig. 2a and b). For the on-site meteorology case, the predicted maximum plume rise (injection height) is 670 m; for the ERA-40 meteorology case, the maximum plume rise is 460 m.

According to the computations with the BUOYANT model, the vertical extents of the plume (lower and upper edges) at the point of maximum plume rise were between 500–800 m (i.e., plume thickness is 300 m) and 200–700 m (plume thickness is 500 m) for the on-site and ERA-40 meteorology cases, respectively. As there were substantial uncertainties both in the determination of the source properties and the relevant

Applicability of an integrated plume rise model

J. Kukkonen et al.

Title Page

Abstract

Introduction

Conclusions

References

Tables

Figures



Back

Close

Full Screen / Esc

Printer-friendly Version

Interactive Discussion



meteorological profiles, we have presented these values only to an accuracy of hundreds of metres.

Hobbs et al. (1996) determined the vertical distribution of smoke particles in the plume from LIDAR measurements on board the Convair aeroplane. The observed injection heights of the aerosol particles ranged from 250 and 600 m according to Trentmann et al. (2002) (shown in Fig. 3). They concluded that the plume was about 400 m thick and it ascended to an average height of about 350 m, as it drifted downwind; the plume was observed to a distance of about 25 km.

The predictions of the BUOYANT model can therefore be considered to be in a fairly good agreement with the observations, taking into account the substantial uncertainties especially in the model input data. In case of on-site meteorology, the model slightly over-predicted the observations; however, this difference could also be caused by the uncertainties in evaluating the fire source term, especially the convective heat flux. There were also substantial differences of the results obtained using the two alternative meteorological datasets.

Also other model evaluations have been previously conducted based on the Quinault fire. Trentmann et al. (2002) simulated the dynamical evolution of the plume, using the active tracer high-resolution atmospheric model (ATHAM). They used as model input the on-site meteorological profiles and the evaluated heat emissions from the fire. They estimated the injection height of the aerosol particles to range from 300 to 700 m (cf. Fig. 3).

Freitas et al. (2007) applied a simple one-dimensional time-dependent entrainment plume model originally developed by Latham (1994) to estimate the plume rise associated with the Quinault prescribed fire. They evaluated that the plume reached a maximum height of about 600 m.

Applicability of an integrated plume rise model

J. Kukkonen et al.

Title Page

Abstract

Introduction

Conclusions

References

Tables

Figures

◀

▶

◀

▶

Back

Close

Full Screen / Esc

Printer-friendly Version

Interactive Discussion



3.1.4 Comparison of the predictions of a semi-empirical model by Sofiev et al. (2012) with measurements

The model of Sofiev et al. (2012) requires as input values the Fire Radiative Power (FRP) of the source, the height of the top of the boundary layer (H_{abl}) and Brunt–Vaisala frequency in the free troposphere (N_{FT}). The evaluation of these input values is based on the data described above. The top of the plume height H_p is evaluated from

$$H_p = \alpha H_{abl} + \beta \left(\frac{FRP}{P_{f_0}} \right)^\gamma \exp \left(-\frac{\delta N_{FT}^2}{N_0^2} \right), \quad (16)$$

where $\alpha = 0.24$, $\beta = 170$ m, $\gamma = 0.35$, $\delta = 0.6$, $P_{f_0} = 10^6$ W and $N_0^2 = 2.4 \times 10^{-4} \text{ s}^{-2}$ (Sofiev et al., 2012).

As FRP, similarly to the sensible heat flux, was not measured directly, we had to assume that it is a certain fraction of the total heat release. Following Wooster et al. (2005), Ichoku and Kaufman (2005), Trentmann et al. (2002) and Sofiev et al. (2009), this fraction was assumed to be 40%; however, the uncertainty of evaluating this fraction is substantial. The maximum FRP was therefore approximately 2.6 GW. Based on the temperature profile observations, assuming the profiles modelled in this study, $H_{abl} = 300$ m.

However, the evaluation of the Brunt–Vaisala frequency is unequivocal. In deriving Eq. (16), it has been assumed that the stability in the free troposphere does not change substantially, which is not the case for the Quinault experiment. Inside the inversion layer, the Brunt–Vaisala frequency $N_{IL}^2 = 7.8 \times 10^{-4} \text{ s}^{-2}$, whereas above it, the Brunt–Vaisala frequency $N_{FT}^2 = 2.5 \times 10^{-4} \text{ s}^{-2}$. Strictly speaking, these conditions are not within the validity regime of Eq. (16). However, that it is the inversion that will mainly restrict the plume rise, not the overlaying layer. Using the value of N_{IL} instead of that of N_{FT} in Eq. (16) results in the top of the plume height $H_p = 450$ m, whereas using the above mentioned value of N_{FT} results in an unrealistic estimate, $H_p = 1.5$ km.

GMDD

7, 483–527, 2014

Applicability of an integrated plume rise model

J. Kukkonen et al.

Title Page

Abstract

Introduction

Conclusions

References

Tables

Figures

◀

▶

◀

▶

Back

Close

Full Screen / Esc

Printer-friendly Version

Interactive Discussion



3.2 The prescribed burning experiment in Hyttälä

3.2.1 Evaluation of the vertical profiles of meteorological variables

Meteorological measurements were carried out on-site at the burn area perimeter, and at the SMEAR II station located 400 m north of the burn area. The measurements at the burn area perimeter were done at the height of 10 m above ground, and the SMEAR II station measurements were done at various heights up to 73 m above ground. The aeroplane measurements were conducted at various heights, the maximum height was about 2.5 km. Measurements on particulate matter on board the aeroplane indicated that at least part of the plume reached the altitude of approximately 1.8 km (Virkkula et al., 2013).

The BUOYANT model requires data on the vertical meteorological profiles at least up to the height of the predicted plume rise. The measurements at the burn area perimeter and the SMEAR II station do not therefore provide sufficient information on the atmospheric vertical profiles. We have additionally applied the measured data from Jokioinen observatory, located approximately 120 km south-southwest of the burn area. Daily sounding data at the observatory of Jokioinen is available at 00:00 and 12:00 UTC.

The vertical wind speed and temperature profiles applied by the model have been presented in Eqs. (3) and (4). As in case of the Quinault experiment, we have evaluated the Monin–Obukhov length using the method presented by Blümel (2000), based on the sounding data at Jokioinen at 12:00 UTC. The estimated value, $L^{-1} = -0.0012 \text{ m}^{-1}$, indicates a moderately unstable condition. Based on the potential temperature profile, the height of the ABL was estimated to be 2250 m. The profiles of potential temperature and wind speed measured at Jokioinen and the modelled profiles are presented in Fig. 4a and b.

Average measured horizontal wind speeds during the flaming phase at the SMEAR station were 0.55 ms^{-1} and 2.2 ms^{-1} at the heights of 8.4 m and 74 m above ground, respectively (Virkkula et al., 2013). The wind speed was light, or it was a calm situation

GMDD

7, 483–527, 2014

Applicability of an integrated plume rise model

J. Kukkonen et al.

Title Page

Abstract

Introduction

Conclusions

References

Tables

Figures

◀

▶

◀

▶

Back

Close

Full Screen / Esc

Printer-friendly Version

Interactive Discussion



during most of the time in the course of the experiment. The corresponding maximum horizontal wind speeds were approximately 2 ms^{-1} and 6 ms^{-1} , respectively, measured on 1 Hz frequency. The BUOYANT -modelled wind speeds were 3.3 ms^{-1} and 4.8 ms^{-1} , correspondingly, at the heights of 8.4 m and 74 m above ground.

5 3.2.2 Evaluation of the source term for the dispersion computations

All the time instants mentioned in the following refer to local time (= UTC +3 h).

The convective heat flux can be determined based on Eqs. (1) and (2), provided that the initial vertical flow velocity, the fire temperature and the ambient temperature are known from measurements. The fire temperature and vertical flow velocity were measured with a sonic anemometer installed in the middle of the burn area at the height of 10 m (Virkkula et al., 2013). The data was measured at a frequency of 10 Hz from 8:00 to 10:39 LT. Unfortunately, as the flaming phase lasted from 8:45 to 11:00 LT, these measured values do not cover the final stages of the flaming phase. The measured ambient air temperature before the burn was approximately 294 K.

The computed convective heat flux density during the flaming phase has been presented in Fig. 5. The substantial temporal variability of the values has been caused partly by the measurement set-up. The fire front advanced from the sides of the burn area towards its centre, in which the sonic anemometer was located. The fire was close to the sensor several times: the first close passage occurred at 09:02–09:11, the second at 09:23–09:26 and the final passage at 09:35–09:52 (Virkkula et al., 2013). After 10:02, the area around the sensor was burning more steadily but with a smaller intensity. The intermittent negative heat flux densities have been caused by downward flow velocities.

As input for the plume rise modelling, we would ideally need spatially representative measurements of the fire temperature and vertical flow speed. This implies that the measurement site for these quantities should ideally be situated in the middle of the formed fire plume at all times. Clearly, this was not possible in the present experimental set-up, as only one permanently positioned site was available in the middle of the

Applicability of an integrated plume rise model

J. Kukkonen et al.

Title Page

Abstract

Introduction

Conclusions

References

Tables

Figures



Back

Close

Full Screen / Esc

Printer-friendly Version

Interactive Discussion



burned area. A practical solution is to select as model input the maximum measured values of the fire temperature and vertical flow speed, either directly from the measured data, or using first a selected temporal averaging of the measured data. A similar approach has also been used in case of the Quinault fire in several previous studies (e.g., Trentmann et al., 2002), and in this study.

We have conducted the model simulations using several alternative heat flux values. We have selected (i) the instantaneous maximum value (this will result in the highest plume rise), and the (ii) maximum one minute average value. An estimate of the source area can be made visually, both (i) based on the photographs taken from the fire, and (ii) by analyzing the measured soil temperatures. We have evaluated a maximum source size to be half of the total burn area, i.e., $A = 0.40$ ha. In order to evaluate the influence of inaccuracy of this estimate, results have also been computed by assuming a substantially smaller area, one fifth of the total burned area. The assumed cases have been presented in Table 1.

3.2.3 Comparison of model results against observations

The measurement data does not allow us to directly estimate the final plume rise. However, the particle number concentration measurements on board the aeroplane provide corresponding information on the ascent of the plume, which can be compared with the predicted centre line trajectory of the plume.

The measured particle number concentrations during the flaming phase (from 09:00 through 09:56), and the predicted trajectories of the plume for the case number 1 have been presented in Fig. 6a and b. We have computed the results by including and excluding the so-called added mass term in Eq. (11), i.e., $k_v = 1$ and $k_v = 0$, respectively. Excluding this term ($k_v = 0$) results in approximately 20% higher predicted plume altitude.

The spatial resolution of the aircraft-based measurements is limited by the lower limit of the aircraft speed. The ground speed of the aeroplane was in the range from 106

Applicability of an integrated plume rise model

J. Kukkonen et al.

Title Page

Abstract

Introduction

Conclusions

References

Tables

Figures

◀

▶

◀

▶

Back

Close

Full Screen / Esc

Printer-friendly Version

Interactive Discussion



to 199 km h^{-1} , yielding a horizontal spatial resolution of approximately 29–55 m for the measured airborne particle number concentration data (Virkkula et al., 2013).

The predictions for cases 1 and 2 agree fairly well with the observations, both assuming $k_v = 1$ and $k_v = 0$. The modelling for the remaining cases 3 and 4 under-predicts the measured plume heights. We expect that the main reason for this under-prediction is the underestimated convective heat flux from the source. This was caused by the measurement set-up that probably during most of the measuring time cannot provide for sufficiently representative values of the potentially very high temperatures and intensive vertical flows in the buoyant plume.

The measured and predicted plume diameters for case number 1 have been compared in Fig. 7. The measured plume widths have been determined based on the measured particle number concentrations on the aeroplane. However, the uncertainty of the measured plume widths is substantial, caused by the limited spatial resolution, especially for the narrowest plumes.

The measured values were defined as the full plume width defined at half of the maximum concentrations (denoted here as FWHM). In more detail, the FWHM is defined as the horizontal distance between two points on a lateral spatial concentration profile, at which the function reaches half its maximum value (Virkkula et al., 2013). The model assumes a top hat profile, which has been converted to an equivalent Gaussian profile using the procedure described in Appendix A.

Similarly to the comparison of the predicted and measured plume altitude values (Fig. 6), the modelled and measured plume diameter values are in a fairly good agreement.

3.2.4 Comparison of the predictions of the BUOYANT model with those of a semi-empirical model

We applied the Eq. (16) in case of the prescribed burn at Hyytiälä. For the four cases defined in Table 1, we obtained the FRP values of 1.6 GW, 0.63 GW, 0.18 GW and

Applicability of an integrated plume rise model

J. Kukkonen et al.

Title Page

Abstract

Introduction

Conclusions

References

Tables

Figures

⏪

⏩

◀

▶

Back

Close

Full Screen / Esc

Printer-friendly Version

Interactive Discussion



69 MW, respectively. Based on the temperature profiles, $H_{abl} = 2300$ m and $N_{FT} = 2.1 \times 10^{-4} \text{ s}^{-2}$. In this case, there are no difficulties in estimating the N_{FT} value. Then the heights of the plume top will be 1.9 km, 1.5 km, 1.2 km and 1.0 km for the cases 1–4, respectively.

4 Conclusions

We have presented an overview of a mathematical model, BUOYANT, that was originally designed for conditions of very high buoyancy, such as might be found in a toxic plume above a major warehouse fire. The model addresses the cross-plume integrated properties of a buoyant plume in the presence of a vertically varying atmosphere, including possibly occurring inversion layers. We have evaluated the validity of the model's application to fires that are much greater than those addressed by the original model. We compared the model predictions with the data of two well-reported prescribed wild-land fire experiments. The model does not contain any free parameters, and was not adjusted to the measured data in any way.

There were substantial differences between the two considered prescribed burning experiments. The burnt area in the Quinault experiment was substantially larger, approximately 20 ha, compared with that in the Hyytiälä experiment, 0.8 ha. Correspondingly, the maximum convective heat flux in the Quinault experiment, 3.6 GW, was clearly higher than that in the Hyytiälä experiment, 0.2 GW (the latter reported here as one minute maximum). The meteorological conditions were also substantially different in these two experiments; there was an elevated inversion in the case of the Quinault experiment. The plume in the Hyytiälä experiment ascended to higher altitudes, compared with that in the Quinault experiment, according to both the measurements and the model predictions. This was mainly caused by the different vertical structure of the atmosphere, especially the temperature inversion in the Quinault case.

For the SCAR-C experiment in Quinault (US) in 1994, the predicted vertical extents of the plume at the point of maximum plume rise were between 500–800 m and 200–

Applicability of an integrated plume rise model

J. Kukkonen et al.

Title Page

Abstract

Introduction

Conclusions

References

Tables

Figures

◀

▶

◀

▶

Back

Close

Full Screen / Esc

Printer-friendly Version

Interactive Discussion



Applicability of an integrated plume rise model

J. Kukkonen et al.

Title Page

Abstract

Introduction

Conclusions

References

Tables

Figures

⏪

⏩

◀

▶

Back

Close

Full Screen / Esc

Printer-friendly Version

Interactive Discussion



700 m for the on-site and ERA-40 meteorology cases, respectively. The observed injection heights of the aerosol particles based on airborne LIDAR measurements ranged from 250 to 600 m, according to Trentmann et al. (2002). Hobbs et al. (1996) evaluated that the plume ascended to an average height of about 350 m, and was about 400 m thick. The predictions can therefore be considered to be in a fairly good agreement with the corresponding observations, taking into account the substantial uncertainties in the model input data. There were substantial differences of the results obtained using two alternative meteorological datasets; this demonstrates the challenges of accurately evaluating the relevant vertical atmospheric profiles.

The BUOYANT model can naturally allow for the variation of the vertical meteorological profiles, and in particular, the influence of the temperature inversions. However, the semi-empirical model of Sofiev et al. (2012) does not have a treatment for low-level inversions. Strictly speaking, it is therefore not applicable in the Quinault case. However, a reasonable agreement of the predictions of this model and measurements was achieved, when the stratification of the inversion layer was taken into account (i.e., the use of N_{IL} instead of N_{FT}).

For the prescribed burning experiment in Hyytiälä (Finland) in 2009, the model predictions were compared with plume elevations and diameters, determined based on number concentration measurements of particulate matter on board an aeroplane. Using maximum measured values of the fire temperature and vertical flow speed as model input values, resulted in a fairly good agreement of modelled and measured results, both regarding the plume trajectories and their diameters. We also evaluated numerically the influence of a maximum variation of one important, but not adequately known model parameter, the factor k_v in the equation for the rate of vertical momentum flux. Its influence was found to be noticeable, but not dominant for the overall results.

There were substantial uncertainties in estimating the source terms for the atmospheric dispersion computations, for both of the addressed prescribed burning experiments. As input values of the plume rise models, we will need to know at least the convective energy release from the fire and the physical extent of the fire. The convective

Applicability of an integrated plume rise model

J. Kukkonen et al.

Title Page

Abstract

Introduction

Conclusions

References

Tables

Figures

◀

▶

◀

▶

Back

Close

Full Screen / Esc

Printer-friendly Version

Interactive Discussion

energy release is the most important source parameter, in terms of the final plume rise. However, the evaluation of the optimally representative convective heat flux includes many uncertainties. For instance, conducting spatially representative measurements of the fire temperatures and vertical flow velocities in the middle of the fire plume throughout the development of a major fire is commonly not possible.

Clearly, there are also uncertainties in the modelling of the plume rise and dispersion. In particular, we have selected to use the form of the entrainment terms according to Ricou and Spalding (1961), instead of the alternative formulation of Morton et al. (1956). However, there is no convincing theoretical or experimental evidence regarding which of these models would be preferable in case of strongly buoyant plume dispersion.

The BUOYANT model contains three numerical parameters that have to be determined based on experimental results (two entrainment coefficients and the k_v factor). We have determined the two plume entrainment coefficients based on wind tunnel measurements by Liedtke and Schatzmann (1997). However, it has not been conclusively shown that the adopted values would be the optimal ones in case of major fires in various atmospheric conditions. The current version of the model assumes a dry atmosphere. However, it has been suggested that the condensation and evaporation of water may possibly play a significant role in plume rise analyses (e.g., Freitas et al., 2007).

5 Code availability

The Fortran 2003 source code of the near and intermediate field dispersion of a highly buoyant plume model is available upon request from the authors. With minor modifications the code can be used also with a Fortran 95 compiler supporting the enhanced data type facilities (ISO/IEC, 1998).

Appendix A

Conversion of the top hat profile of the concentration to an equivalent Gaussian profile

Integral models of buoyant plumes assume that the plume can be described by bulk representations of the flow, varying with distance along the plume centre line, such as plume velocity, density, concentration and other properties. Martin et al. (1997) have examined the possible existence of a buoyant plume to have a self-similar flow. A field ϕ (velocity, density, etc.) is defined here to be self-similar, if it is separable in the form

$$\phi(s, r) = \phi_s(s)\phi_r(r), \quad (\text{A1})$$

where s is the distance along the plume centre line and r is the radial distance from the centre of the plume. Martin et al. (1997) concluded that in principle the three dimensional Reynolds equations (reduced to two dimensions by the assumption of cylindrical symmetry) have a limited form of self-similarity. Self-similar solutions may be a reasonable expectation in many cases, but only after some specified distance from source (Fanneløp and Webber, 2003).

For simplicity, let us assume first an isothermal plume, i.e., the temperature outside of the plume is the same as the temperature within the plume. Let us also assume that wind speed is the only atmospheric property that varies with height. We assume a Gaussian distribution for concentration and wind speed inside the plume of the form

$$\begin{aligned} c(s, r) &= c_s(s)e^{-(r/R_s)^2}, \\ u(s, r) &= u_s(s)e^{-\lambda(r/R_s)^2}, \end{aligned} \quad (\text{A2})$$

where R_s is the Gaussian radius of the plume and the factor λ allows the concentration and wind speed profiles to have different Gaussian radii. Martin et al. (1997) provided an analytical solution for c_s , R_s and u_s in terms of the plume top hat quantities.

GMDD

7, 483–527, 2014

Applicability of an integrated plume rise model

J. Kukkonen et al.

Title Page

Abstract

Introduction

Conclusions

References

Tables

Figures

◀

▶

◀

▶

Back

Close

Full Screen / Esc

Printer-friendly Version

Interactive Discussion



However, for more realistic non-isothermal plume within varying atmosphere, it is not possible for the concentration, and excess temperature and density to be all self-similar (Martin et al., 1997, p. 179). Our procedure here is therefore to apply a simpler method, suitably modified from the method presented by Jagger (1983), where only the radial concentration distribution has a Gaussian distribution (all other fields are assumed to have a top hat profile). The radial concentration distribution is then given by

$$c(s, r) = c_g(s)e^{-(r/\sigma)^2}, \quad (\text{A3})$$

where c_g is the maximum concentration of the Gaussian distribution.

The top hat radius (R) of the plume is defined by the 10% of the peak Gaussian concentration distribution, i.e. $\sigma^2 = R^2/\ln(10)$. Half of the maximum Gaussian concentration therefore occurs at

$$r = \sqrt{\frac{\ln(2)}{\ln(10)}}R \approx 0.55R. \quad (\text{A4})$$

The maximum concentration of the Gaussian distribution can be determined by equating the radially integrated top hat and Gaussian distributions from zero to infinity (i.e. conserving the mass flux), yielding

$$c_g(s) = \sqrt{\frac{\ln(10^4)}{\pi}}c_m(s) \approx 1.71c_m(s), \quad (\text{A5})$$

where $c_m(s)$ is the top-hat concentration.

Acknowledgements. We wish to thank Jörg Trentmann of the Deutscher Wetterdienst for the availability of the measured data on board the Convair aeroplane. Support of the Academy of Finland project ASTREX, as well as that of the FP7 projects TRANSPHORM and PEGASOS is acknowledged.

References

- Beljaars, A. C. M. and Holtslag, A. A. M.: Flux parameterization over land surfaces for atmospheric models, *J. Appl. Meteorol.*, 30, 327–341, 1991.
- Blümel, K.: An approximate analytical solution of flux-profile relationships for the atmospheric surface layer with different momentum and heat roughness lengths, *Bound.-Lay. Meteorol.*, 97, 251–271, 2000.
- Briggs, G. A.: Plume rise predictions, in: *Lectures on Air Pollution and Environmental Impact Analyses*, edited by: Haugen, D. A., American Meteorological Society, Boston, 59–111, 1975.
- Brutsaert, W.: *Evaporation Into the Atmosphere*, D. Riedel Publishing Company, Dordrecht, 299 pp., 1982.
- Davison, P. S.: Estimating the direct radiative forcing due to haze from the 1997 forest fires in Indonesia, *J. Geophys. Res.*, 109, 1–12, 2004.
- Devenish, B. J., Rooney, G. G., Webster, H. N., and Thomson, D. J.: The entrainment rate for buoyant plumes in a crossflow, *Bound.-Layer Meteorol.*, 134, 411–439, 2010.
- Diner, D. J., Beckert, J. C., Reilly, T. H., Bruegge, C. J., Conel, J. E., Kahn, R. A., Martonchik, J. V., Ackerman, T. P., Davies, R., Gerstl, S. A. W., Gordon, H. R., Muller, J.-P., Myneni, R. B., Sellers, P. J., Pinty, B., and Verstraete, M. M.: Multi-angle Imaging SpectroRadiometer (MISR) instrument description and experiment overview, *IEEE T. Geosci. Remote.*, 36, 1072–1087, 1998.
- ERA 40: Daily Fields, available at http://data-portal.ecmwf.int/data/d/era40_daily/, last access: 29 October 2013.
- Fanneløp, T. K. and Webber, D. M.: On buoyant plumes rising from area sources in a calm environment, *J. Fluid Mech.*, 497, 319–334, 2003.
- Fisher, B. E. A., Metcalfe, E., Vince, I., and Yates, A.: Modelling plume rise and dispersion from pool fires, *Atmos. Environ.*, 35, 2101–2110, 2001.
- Forster, C., Wandinger, U., Wotawa, G., James, P., Mattis, I., Althausen, D., Simmonds, P., O'Doherty, S., Jennings, S. G., Kleefeld, C., Schneider, J., Trickl, T., Kreipl, S., Jäger, H., and Stohl, A.: Transport of boreal forest fire emissions from Canada to Europe, *J. Geophys. Res.*, 106, 22887–22906, 2001.
- Freitas, S. R., Longo, K. M., Chatfield, R., Latham, D., Silva Dias, M. A. F., Andreae, M. O., Prins, E., Santos, J. C., Gielow, R., and Carvalho Jr., J. A.: Including the sub-grid scale

GMDD

7, 483–527, 2014

Applicability of an integrated plume rise model

J. Kukkonen et al.

Title Page

Abstract

Introduction

Conclusions

References

Tables

Figures

◀

▶

◀

▶

Back

Close

Full Screen / Esc

Printer-friendly Version

Interactive Discussion



Applicability of an integrated plume rise model

J. Kukkonen et al.

Title Page

Abstract

Introduction

Conclusions

References

Tables

Figures

◀

▶

◀

▶

Back

Close

Full Screen / Esc

Printer-friendly Version

Interactive Discussion



plume rise of vegetation fires in low resolution atmospheric transport models, *Atmos. Chem. Phys.*, 7, 3385–3398, doi:10.5194/acp-7-3385-2007, 2007.

Garratt, J. R.: The atmospheric boundary layer, Cambridge University Press, Cambridge, 316 pp., 1994.

5 Gassó, S. and Hegg, D. A.: Comparison of columnar aerosol optical properties measured by the MODIS airborne simulator with in situ measurements: a case study, *Remote Sens. Environ.*, 66, 138–152, 1998.

Gear, C. W.: Numerical initial value problems in ordinary differential equations, Prentice-Hall, Inc. Englewood Cliffs, New Jersey, 253 pp., 1971.

10 Hari, P. and Kulmala, M.: Station for measuring ecosystem-atmosphere relations (SMEAR II), *Boreal Environ. Res.*, 10, 315–322, 2005.

Hobbs, P. V., Reid, J. S., Herring, J. A., Nance, J. D., Weiss, R. E., Ross, J. L., Hegg, D. A., Ottmar, R. D., and Liousse, C.: Particle and trace-gas measurements in the smoke from prescribed burns of forest products in the Pacific Northwest, in: *Biomass Burning and Global Change*, edited by: Levine, J. S., MIT Press, Cambridge, MA, 697–715, 1996.

15 Ichoku, C. and Kaufman, Y. J.: A method to derive smoke emission rates from MODIS fire radiative energy measurements, *IEEE T. Geosci. Remote*, 43, 2636–2649, 2005.

ISO/IEC: Information technology – Programming languages – Fortran – Enhanced data type facilities, Technical Report ISO/IEC 15581:1998, 1998.

20 Jagger, S. F.: Development of CRUNCH: A dispersion model for continuous releases of denser-than-air vapour into the atmosphere, UKAEA Report SRD R 229, Safety and Reliability Directorate, Warrington, 26 pp. + app., 1983.

Jirka, G. H.: Integral model for turbulent buoyant jets in unbounded stratified flows, Part I: Single round jet, *Environ. Fluid Mech.*, 4, 1–56, 2004.

25 Kaufman, Y. J., Remer, L. A., Ottmar, R. D., Ward, D. E., Li, R.-R., Kleidman, R., Fraser, R. S., Flynn, L., McDougal, D., and Shelton, G.: Relationship between remotely sensed fire intensity and rate of emission of smoke: SCAR-C experiment, in: *Biomass Burning and Global Change*, edited by: Levine, J. S., MIT Press, Cambridge, MA, 685–696, 1996.

30 Kukkonen, J., Nikmo, J., Ramsdale, S. A., Martin, D., Webber, D. M., Schatzmann, M., and Liedtke, J.: Dispersion from strongly buoyant sources, in: *Air Pollution Modeling and its Application XIII*, edited by: Gryning, S.-E. and Batchvarova, E., Kluwer Academic/Plenum Publishers, 539–547, 2000.

Applicability of an integrated plume rise model

J. Kukkonen et al.

Title Page

Abstract

Introduction

Conclusions

References

Tables

Figures

⏪

⏩

◀

▶

Back

Close

Full Screen / Esc

Printer-friendly Version

Interactive Discussion



- Kulmala, M., Asmi, A., Lappalainen, H. K., Carslaw, K. S., Pöschl, U., Baltensperger, U., Hov, Ø., Brenquier, J.-L., Pandis, S. N., Facchini, M. C., Hansson, H.-C., Wiedensohler, A., and O'Dowd, C. D.: Introduction: European Integrated Project on Aerosol Cloud Climate and Air Quality interactions (EUCAARI) – integrating aerosol research from nano to global scales, *Atmos. Chem. Phys.*, 9, 2825–2841, doi:10.5194/acp-9-2825-2009, 2009.
- Latham, D.: PLUMP: A one-dimensional plume predictor and cloud model for fire and smoke managers, General Technical Report INT-GTR-314, Intermountain Research Station, USDA Forest Service, 15 pp., 1994.
- Liedtke, J. and Schatzmann, J.: Dispersion of plumes from strongly buoyant sources, Final Report to EC under contract EV5V-CT93-0262, 125 pp., 1997.
- Liousse, C., Penner, J. E., Chuang, C., Walton, J. J., Eddleman, H., and Cachier, H.: A global three-dimensional model study of carbonaceous aerosols, *J. Geophys. Res.*, 101, 19411–19432, 1996.
- Martin, D., Webber, D. M., Jones, S. J., Underwood, B. Y., Tickle, G. A., and Ramsdale, S. A.: Near- and intermediate-field dispersion from strongly buoyant sources, AEA Technology Report AEAT/1388, Warrington, 277 pp., 1997.
- Mazzoni, D., Logan, J. A., Diner, D., Kahn, R., Tong, L., and Li, Q.: A data-mining approach to associating MISR smoke plume heights with MODIS fire measurements, *Remote Sens. Environ.*, 107, 138–148, 2007.
- Menzel, W. P. and Prins, E. M.: Monitoring biomass burning with the new generation of geostationary satellites, in: *Biomass Burning and Global Change*, edited by: Levine, J. S., MIT Press, Cambridge, MA, 56–64, 1996.
- Middleton, J. H.: The rise of forced plumes in a stably stratified crossflow, *Bound.-Lay. Meteorol.*, 36, 187–199, 1986.
- Morton, B. R., Taylor, G., and Turner, J. S.: Turbulent gravitational convection from maintained and instantaneous sources, *P. R. Soc. A*, 234, 1–23, 1956.
- Nikmo, J., Tuovinen, J.-P., Kukkonen, J., and Valkama, I.: A hybrid plume model for local-scale dispersion, *Publications on Air Quality 27*, Finnish Meteorological Institute, Helsinki, 65 pp., 1997.
- Nikmo, J., Tuovinen, J. P., Kukkonen, J., and Valkama, I.: A hybrid plume model for local-scale atmospheric dispersion, *Atmos. Environ.*, 33, 4389–4399, 1999.
- Olesen, H. R.: Datasets and protocol for model validation, *Int. J. Environ. Pollut.*, 5, 693–701, 1995.

Applicability of an integrated plume rise model

J. Kukkonen et al.

Title Page

Abstract

Introduction

Conclusions

References

Tables

Figures

◀

▶

◀

▶

Back

Close

Full Screen / Esc

Printer-friendly Version

Interactive Discussion



- Paulson, C. A.: The mathematical representation of wind speed and temperature profiles in the unstable atmospheric surface layer, *J. Appl. Meteorol.*, 9, 857–861, 1970.
- Ramsdale, S. A., Martin, D., Nikmo, J., Kukkonen, J., Liedtke, J., and Schatzmann, M.: Dispersion from strongly buoyant sources – overall executive summary, AEA Technology Report AEAT/1408, Warrington, 16 pp., 1997.
- Ricou, F. P. and Spalding, D. B.: Measurement of entrainment by axisymmetrical turbulent jets, *J. Fluid Mech.*, 11, 21–32, 1961.
- Sandberg, D. V. and Peterson, J.: A source strength model for prescribed fire in coniferous logging slash, in: Proceedings of the 21st annual meeting of the Air Pollution Control Association, 12–14 November 1984, Portland, Oregon, 10 pp., 1984.
- Schobesberger, S., Väänänen, R., Leino, K., Virkkula, A., Backman, J., Pohja, T., Siivola, E., Franchin, A., Mikkilä, J., Paramonov, M., Aalto, P. P., Krejci, R., Petäjä, T., and Kulmala, M.: Airborne measurements over the boreal forest of southern Finland during new particle formation events in 2009 and 2010, *Boreal Environ. Res.*, 18, 145–163, 2013.
- SLATEC: Common Mathematical Library, available at: <http://www.netlib.org/slatec/index.html>, last access: 29 October 2013.
- Sofiev, M., Vankevich, R., Lotjonen, M., Prank, M., Petukhov, V., Ermakova, T., Koskinen, J., and Kukkonen, J.: An operational system for the assimilation of the satellite information on wild-land fires for the needs of air quality modelling and forecasting, *Atmos. Chem. Phys.*, 9, 6833–6847, doi:10.5194/acp-9-6833-2009, 2009.
- Sofiev, M., Ermakova, T., and Vankevich, R.: Evaluation of the smoke-injection height from wild-land fires using remote-sensing data, *Atmos. Chem. Phys.*, 12, 1995–2006, doi:10.5194/acp-12-1995-2012, 2012.
- Trentmann, J., Andreae, M. O., Graf, H.-F., Hobbs, P. V., Ottmar, R. D., and Trautmann, T.: Simulation of a biomass-burning plume: comparison of model results with observations, *J. Geophys. Res.*, 107, AAC5.1–AAC5.15, doi:10.1029/2001JD000410, 2002.
- Uppala, S. M., Kållberg, P. W., Simmons, A. J., Andrae, U., Da Costa Bechtold, V., Fiorino, M., Gibson, J. K., Haseler, J., Hernandez, A., Kelly, G. A., Li, X., Onogi, K., Saarinen, S., Sokka, N., Allan, R. P., Andersson, E., Arpe, K., Balmaseda, M. A., Beljaars, A. C. M., Van De Berg, L., Bidlot, J., Bormann, N., Caires, S., Chevallier, F., Dethof, A., Dragosavac, M., Fisher, M., Fuentes, M., Hagemann, S., Hólm, E., Hoskins, B. J., Isaksen, I., Janssen, P. A. E. M., Jenne, R., McNally, A. P., Mahfouf, J.-F., Morcrette, J.-J., Rayner, N. A.,

Applicability of an integrated plume rise model

J. Kukkonen et al.

Title Page

Abstract

Introduction

Conclusions

References

Tables

Figures

◀

▶

◀

▶

Back

Close

Full Screen / Esc

Printer-friendly Version

Interactive Discussion



- Saunders, R. W., Simon, P., Sterl, A., Trenberth, K. E., Untch, A., Vasiljevic, D., Viterbo, P., and Woollen, J.: The ERA-40 re-analysis, *Q. J. Roy. Meteor. Soc.*, 131, 2961–3012, 2005.
- van Ulden, A. P. and Holtstlag, A. A. M.: Estimation of atmospheric boundary layer parameters for diffusion applications, *J. Climate Appl. Meteor.*, 24, 1196–1207, 1985.
- 5 Virkkula, A., Levula, J., Pohja, T., Aalto, P. P., Keronen, P., Schobesberger, S., Clements, C. B., Pirjola, L., Kieloaho, A.-J., Kulmala, L., Aaltonen, H., Patokoski, J., Pumpanen, J., Rinne, J., Ruuskanen, T., Pihlatie, M., Manninen, H. E., Aaltonen, V., Junninen, H., Petäjä, T., Backman, J., Dal Maso, M., Nieminen, T., Olsson, T., Grönholm, T., Kerminen, V.-M., Schultz, D. M., Kukkonen, J., Sofiev, M., de Leeuw, G., Bäck, J., Hari, P., and Kulmala, M.:
 10 Overview of a prescribed burning experiment within a boreal forest in Finland, *Atmos. Chem. Phys. Discuss.*, 13, 21703–21763, doi:10.5194/acpd-13-21703-2013, 2013.
- Wigley, T. M. L. and Slawson, P. R.: On the condensation of buoyant, moist, bent-over plumes, *J. Appl. Meteorol.*, 10, 253–259, 1971.
- 15 Wooster, M. J., Roberts, G., Perry, G. L. W., and Kaufman, Y. J.: Retrieval of biomass combustion rates and totals from fire radiative power observations: FRP derivation and calibration relationships between biomass consumption and fire radiative energy release, *J. Geophys. Res.*, 110, doi:10.1029/2005JD006318, D24311, 2005.

Applicability of an integrated plume rise model

J. Kukkonen et al.

Title Page

Abstract

Introduction

Conclusions

References

Tables

Figures

◀

▶

◀

▶

Back

Close

Full Screen / Esc

Printer-friendly Version

Interactive Discussion



Table 1. The definition of the example cases selected for the prescribed burning experiment in Hyytiälä, and the computed convective heat fluxes (Q_c) for these cases. The computations were performed for the measured maximum values and for measured maximum values during one minute for the fire temperatures (T) and the measured vertical flow velocities (v). Two alternative values were assumed for the measured active fire source areas (A), for each averaging option.

Case number	Averaging of T , v and Q_c	T (K)	v (m s^{-1})	A (ha)	Q_c (MW)
1	Instantaneous maximum	370	7.3	0.40	2200
2	Instantaneous maximum	370	7.3	0.16	870
3	Maximum during one minute	310	3.2	0.40	240
4	Maximum during one minute	310	3.2	0.16	95

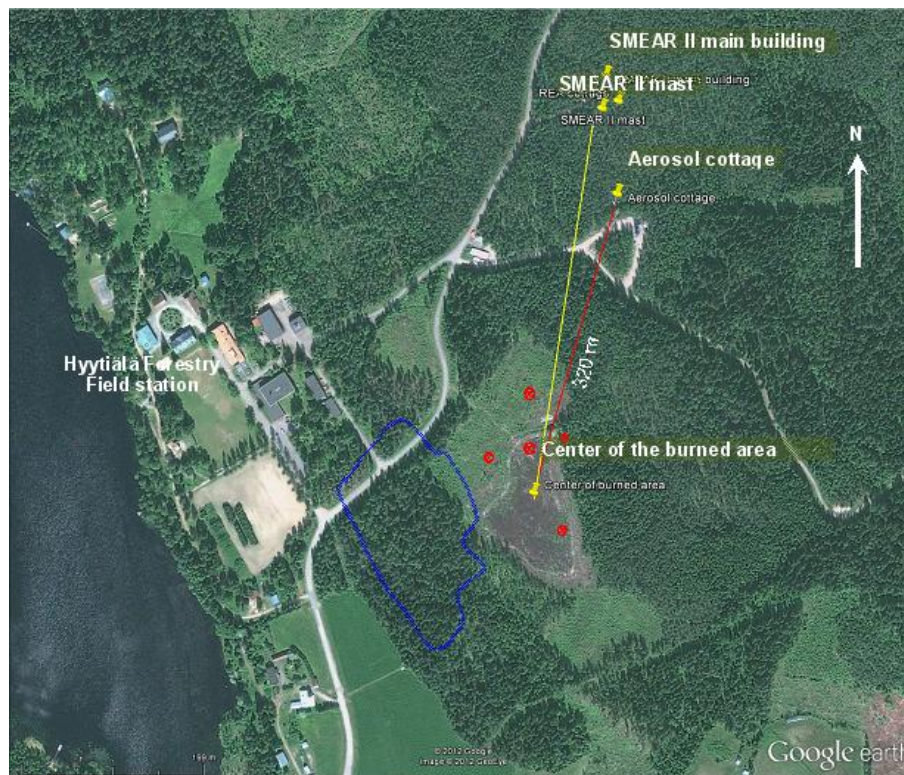


Fig. 1. Location of the burned area (in grey), the SMEAR II main building, mast, and aerosol cottage (yellow pins), and the meteorological measurements within and around the burning area (red dots). The distance from the centre of the burned area to the aerosol cottage is 320 m. The blue line encircles a non-burned reference area. This Google Earth satellite image was taken on 4 July 2010, approximately a year after the burn.

Applicability of an integrated plume rise model

J. Kukkonen et al.

[Title Page](#)

[Abstract](#) [Introduction](#)

[Conclusions](#) [References](#)

[Tables](#) [Figures](#)

[◀](#) [▶](#)

[◀](#) [▶](#)

[Back](#) [Close](#)

[Full Screen / Esc](#)

[Printer-friendly Version](#)

[Interactive Discussion](#)



Applicability of an integrated plume rise model

J. Kukkonen et al.

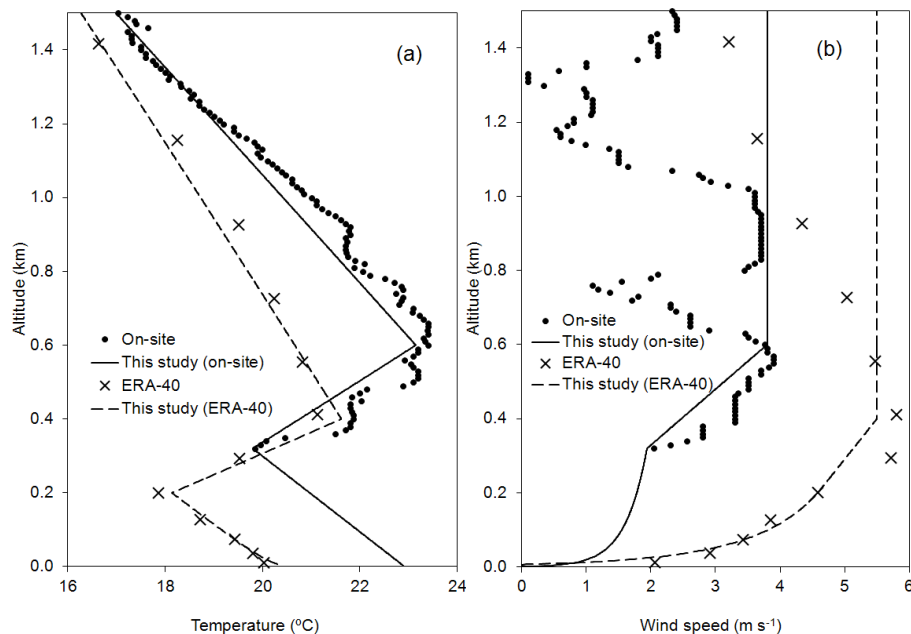


Fig. 2. Vertical profiles of temperature and wind speed measured on-site on board the Convair aeroplane (dots), the ERA-40 analysed data (crosses), and the corresponding modelled profiles in this study (solid and dashed lines) for the Quinault field experiment.

Title Page

Abstract

Introduction

Conclusions

References

Tables

Figures

◀

▶

◀

▶

Back

Close

Full Screen / Esc

Printer-friendly Version

Interactive Discussion



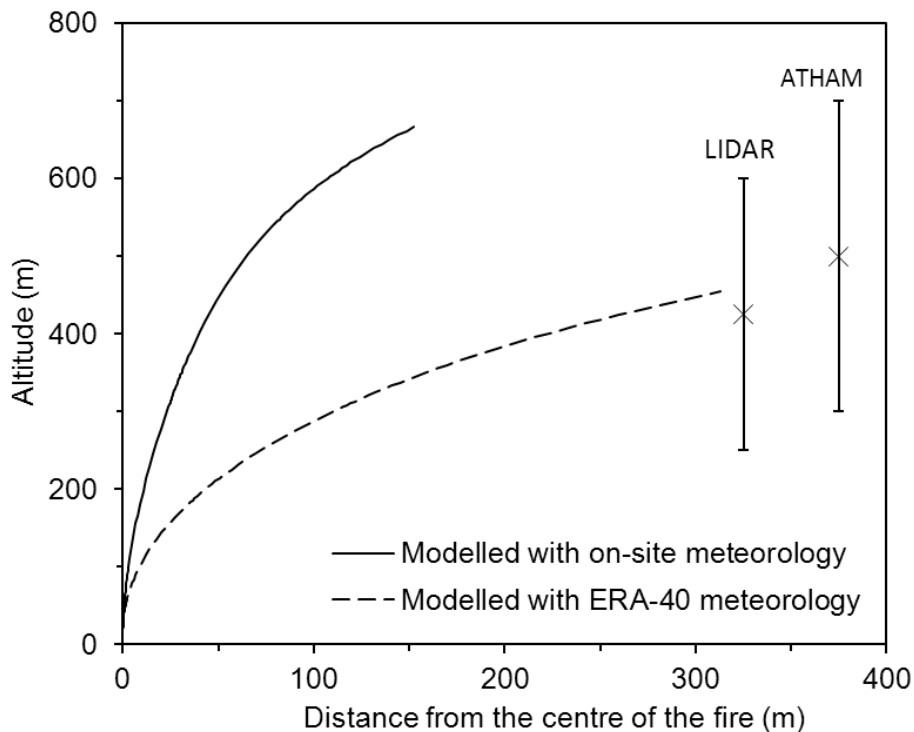


Fig. 3. Simulated altitude of the centre line of the plume for the Quinault prescribed burn as a function of the downwind distance. The results are shown both for using (i) the meteorological measurements made on site (denoted by “on-site meteorology”) and (ii) the re-analysis of the meteorological observations (“ERA-40 meteorology”). The vertical ranges of the previous results obtained using on-site LIDAR measurements (“LIDAR”; Trentmann et al., 2002) and computations using the ATHAM model (Trentmann et al., 2002) have also been presented.

Applicability of an integrated plume rise model

J. Kukkonen et al.

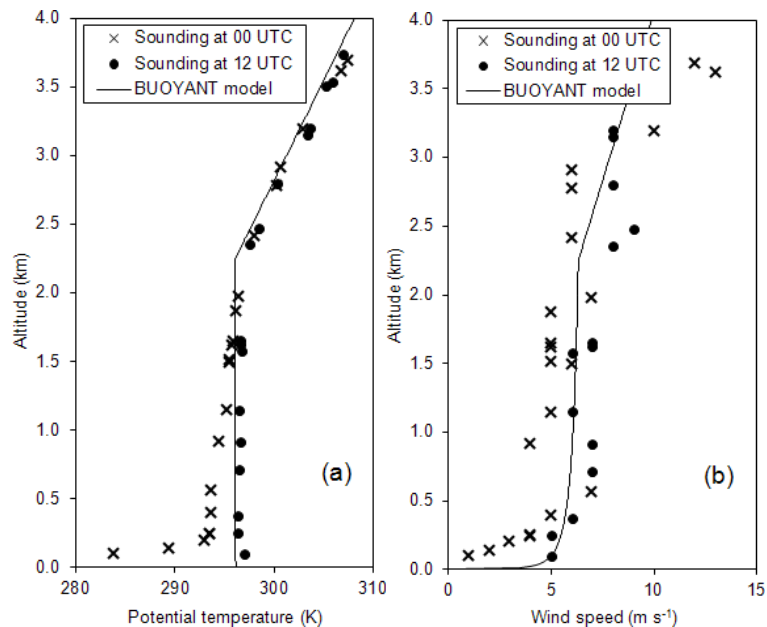


Fig. 4. Vertical profiles of potential temperature and wind speed, both measured at the observatory of Jokioinen on 26 June 2009 at 00:00 and 12:00 UTC, and the modelled profiles at 12:00 UTC.

[Title Page](#)[Abstract](#)[Introduction](#)[Conclusions](#)[References](#)[Tables](#)[Figures](#)[◀](#)[▶](#)[◀](#)[▶](#)[Back](#)[Close](#)[Full Screen / Esc](#)[Printer-friendly Version](#)[Interactive Discussion](#)

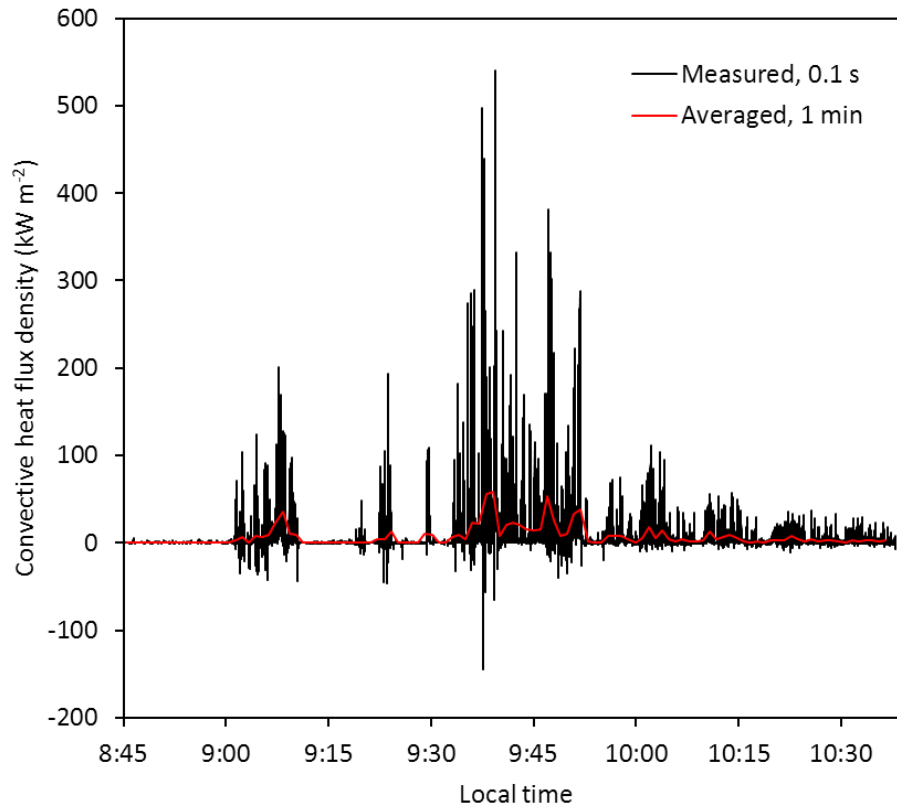


Fig. 5. Computed convective heat flux density, determined from measurements during most of the flaming phase (black line). The measuring frequency was 10Hz. The one minute average value of the convective heat flux density is also presented (red line).

Applicability of an integrated plume rise model

J. Kukkonen et al.

Title Page

Abstract

Introduction

Conclusions

References

Tables

Figures

◀

▶

◀

▶

Back

Close

Full Screen / Esc

Printer-friendly Version

Interactive Discussion



Applicability of an integrated plume rise model

J. Kukkonen et al.

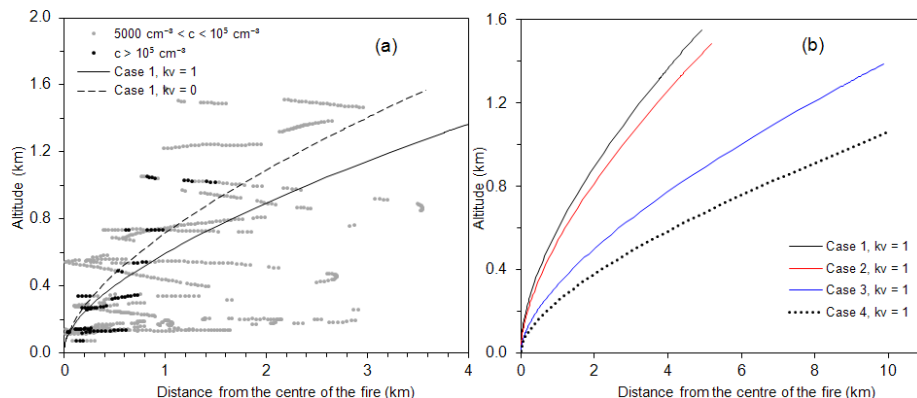


Fig. 6. (a) Total particle number concentrations measured on an aircraft in Hyytiälä during the flaming stage on 26 June 2009 (grey and black dots), and the predicted plume centre line trajectory for case 1, assuming $k_v = 1$ and $k_v = 0$ (Eq. 11). The measured particle number concentrations (c) have been classified to two separate categories: highest (black dots) and medium high (grey dots) concentrations (the ranges are indicated in the figure caption). The particle number concentrations were determined for particles having an aerodynamical diameter larger than 3 nm. (b) The predicted plume centre line trajectories for cases 1–4, assuming $k_v = 1$. The horizontal axes of the (a) and (b) are different.

Title Page

Abstract

Introduction

Conclusions

References

Tables

Figures

◀

▶

◀

▶

Back

Close

Full Screen / Esc

Printer-friendly Version

Interactive Discussion



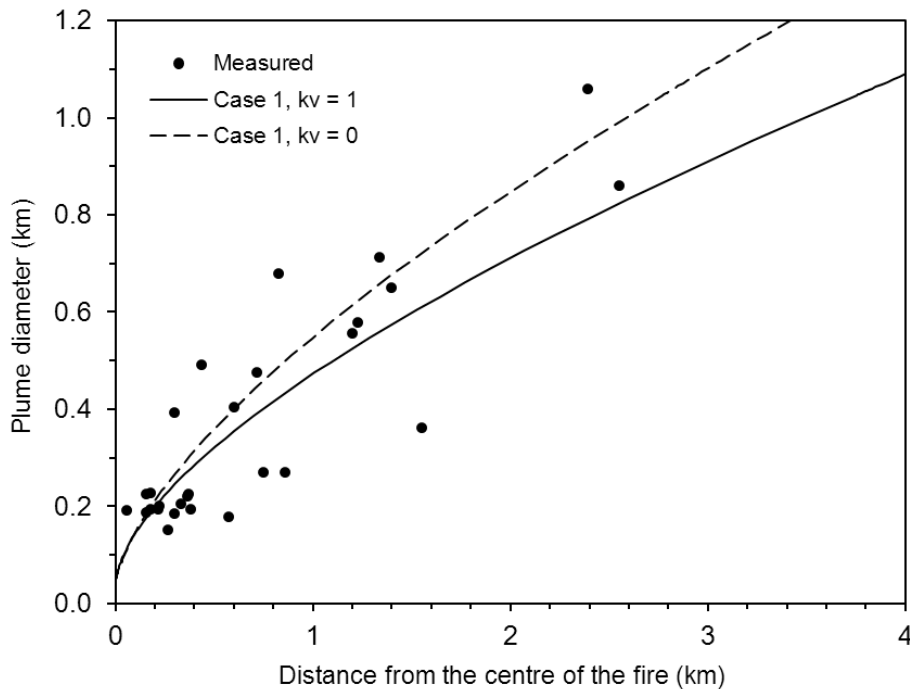


Fig. 7. The measured and predicted plume diameters against downwind distance from the centre of the fire, for case number 1. The data of measurements are presented as black dots, and predictions as solid and dotted lines.